J Solid State Electrochem (2012) 16:2541–2546
DOI 10.1007/s10008-012-1657-z

ORIGINAL PAPER

Investigation of the electrode molding technologies for the carbon-based supercapacitors

Kedi Cai · Weifang Mu · Tieshi He · Junbo Hou

Received: 12 August 2011 / Revised: 11 January 2012 / Accepted: 14 January 2012 / Published online: 17 February 2012

Abstract In this study, we investigated the influence of electrode molding pressure, temperature, and time on the properties of the winding supercapacitors. Mechanical properties such as the crook degree and adhesion strength of the formed electrodes were tested. The electrochemical performance of a supercapacitor was examined using an AC impedance, cyclic voltammetry, and constant current charging/discharging tests. According to the results, at 20-MPa electrode molding pressure and 80 °C for 60 s, the supercapacitor showed the best performances with its electrochemical window reaching 4.4 V, a charge–discharge efficiency of 97.6%, and a specific capacitance of 370.0 Fg^{-1}.

Keywords Supercapacitor · Electrode · Molding technologies

Introduction

The supercapacitor is a relatively new electrochemical energy storage device that acts as both a traditional capacitor and a storage battery [1]. Its numerous advantages include fine pulse performance, quick discharge, nonpollution, low maintenance requirement, and long lifespan. It has been gaining popularity as a source of environment-friendly energy [2–5] and has become a great candidate in the applications like aviation and space, defense and military industry, electric-powered vehicles, wireless communication, and consumer electronic products [6–8].

Active carbon has merits such as low cost and stable chemical properties, making it the most widely used material for the electrodes of the supercapacitors. Whether active carbon electrodes with fine properties could be made is therefore significant and decisive. With respect to the state of art for the supercapacitor electrode manufacturing technologies, it still requires further detail investigations on the key technologies of pole piece coating and molding [9–11]. The commercial electrodes were purchased for some cases and then cut, wound, and encapsulated to manufacture the desired devices, but this dramatically increases cost. For some cases active carbon fabric was directly adopted as electrode material for water purification so as to evade the pole piece coating process [12–15]. However, electrodes made through this method usually have weak mechanical strength and low cubic volume. A limited number of enterprises that research, develop, and manufacture electrode independently encounter a lot of problems such as low conductivity, low specific capacity, high internal resistance, big capacity loss, poor recycling property, and easy fall off of active substances. It is therefore realistic and crucial to improve the properties of supercapacitors when conducting research on manufacturing and molding techniques [16] of the active carbon electrode, specifically the formula of the active substance on the pole piece, the selection of the adhesion agent system, the manufacturing techniques, as well as the aging mechanism. The aim of this research is to investigate the manufacturing techniques by producing an

K. Cai (✉) · W. Mu · T. He
Institute of Liaoxi Ecological Environment Science,
Bohai University,
Jinzhou 121013, China
e-mail: caikedihit@tsinghua.edu.cn

K. Cai
Institute of Nuclear and New Energy Technology,
Tsinghua University,
Beijing 100084, China

J. Hou
Institute for Critical Technology and Applied Science,
Virginia Tech,
Blacksburg, VA 24061, USA

organic winding supercapacitor. Self-made active carbon was taken as the raw material; controlled pole piece molding temperature, pressure, and rolling time, which were inherent in the pole piece manufacturing process, were also studied. In addition, an optimization research was made on the technical parameters. The properties of the capacitor under optimization conditions were probed to make clear the magnitude of influence of the technological parameters on electrode performance [17, 18] and consequently confirm the best manufacturing technology for the supercapacitor electrode.

Experimental

Preparation of electrode

The electrode preparation process for supercapacitor is shown in Fig. 1. Active carbon powder (HY-100; Caoyang, China), the surface area of active carbon, is 1,300 $m^2\ g^{-1}$, and the pore size distribution active carbon ranges from 0.1 to 50 nm and most of the pores are around 3 nm. Conductive additive (graphite powder), dispersant (ethanol), thickening agent (sodium salt of caboxymethyl cellulose), and adhesion agent (polytetrafluoroethylene, mass ratio 78:10:2:2:8) were mixed and blended until the mixture was free of particles. The mixture slurry was then laid evenly onto aluminum sheets with a spreader, and the coated sheets were dried up in the oven. The electrodes were hot pressed under various pressures, temperatures, and times. The various hot pressing conditions of the electrodes are shown in Table 1. The coated sheets were then placed in a vacuum drying oven for 8–12 h to finally obtain the active carbon electrodes.

Fabrication of supercapacitor

The working (thickness 40 μm, size 9×50 mm) and auxiliary electrodes (120 μm, size 12.5×65 mm) used in this work were activated carbon electrode. A silver wire was used as the reference electrode. The working, auxiliary, and reference electrodes were placed into the glove box filled with dry nitrogen for drying for 6 h. These are then stacked together in sequence and then turned into cores after tight winding. The wound up cores were placed into the electrolyte and then in a vacuum for 1 h. Next, up to 10 mL of triethylmethylammonium tetrafluoroborate/glutaronitrile (1 mol L^{-1}) electrolytes were added, and these were assembled into a supercapacitor after encapsulation.

Measuring electrode compression ratio, crook degree, and adhesion

The mechanical properties of the electrodes are shown in Table 1. The thickness of AC electrode was measured by a paint film thickness gauge (QUJ, Glmgs, China). Subsequently, the compression ratio of the pole piece was obtained from the difference between the pre- and the post-dried films. The bending strength of the AC electrode was measured by the film cylindrical bending tester (QTY-32, Tjjingke, China). The diameters of the axial bars were 2, 6, 8, 10, 12, 16, 18, 20, 25, and 32 mm. The AC electrode should meet the requirement that at the minimum diameter of axial bar, the AC electrode did not crack when it was bent 180° around the axial bar for 3 s. The adhesion strength of the AC electrode was measured by a film adhesion tester (QFZ, Glmgs, China), and the evaluation can be divided into seven grades according to the rolling line scratch, from which the grade 1 showed the strongest adhesion and grade 7 indicated the weakest.

Electrochemical measurements

A Princeton Applied Research Model VSP electrochemical workstation was used to measure the electrochemical performance of the supercapacitor. AC impedance was tested using the following parameters: AC signals amplitude was 5 mV; frequency range was 0.05~200 kHz. Cyclic voltammetry was tested at the scanning rate of 5 mV s^{-1}. Constant current charging/discharging was tested at the current of 200 mA.

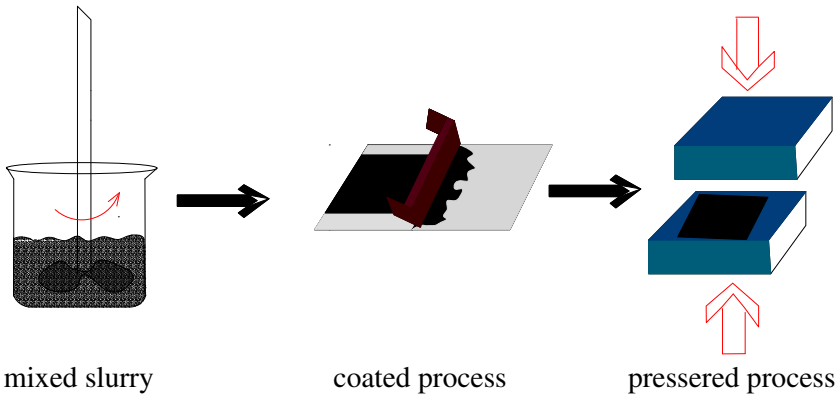

Fig. 1 Preparation process of electrodes for supercapacitor

Table 1 The various hot pressing conditions and the properties of the electrodes

Electrodes	Pressure (MPa)	Temperature (°C)	Time (s)	Compression ratio (%)	Degree of crook (mm)	Adhesive force (level)
EP_1	5	80	60	8.4	12	6
EP_2	10	80	60	12.6	10	6
EP_3	15	80	60	17.4	8	4
EP_4	20	80	60	19.3	4	2
EP_5	25	80	60	21.9	5	2
ET_6	20	25	60	19.1	12	4
ET_7	20	50	60	19.6	8	4
ET_8	20	100	60	20.5	3	3
ET_9	20	120	60	20.8	3	3
Et_{10}	20	80	30	13.6	6	4
Et_{11}	20	80	120	23.2	5	2

Results and discussion

Influence of electrode molding pressure

The electrodes manufactured under different pressures were assembled into supercapacitors, and then the electrochemical tests were conducted. The functional parameters of the capacitors such as mass ratio capacity, volume ratio capacity, energy density, maximum power density, direct current internal resistance, and charge–discharge efficiency were calculated (Table 2) in accordance with the constant current charge–discharge curve of the supercapacitor [19]. At 20 MPa pole piece molding pressure, the supercapacitor exhibits the best performance, with 97.6% charge–discharge efficiency, and 370.0 Fg^{-1} mass ratio volume.

Electrode molding pressure is an important factor that influences specific capacity: a bigger pressure is beneficial for tight contact between the electrode material and the current collector, but this reduces electrical resistance. On the other hand, excess pressure will cause too much compaction of the partial holes of the active carbon and blockade, and this fends off the electrolyte. Consequently, the material utilization rate will drop and the specific electrical capacity will decrease. As the molding pressure goes up, the internal resistance goes down. Above 20 MPa, the resistance slightly increases (Table 2), indicating full contact between active carbons under this pressure. The specific capacity increases in the ranges of the molding pressure 5–20 MPa. When the molding pressure is up to 25 MPa, the specific capacity levels off. The fact that above 20 MPa the specific capacity drops quickly indicates that the compaction ratio of active carbon holes is too high at high pressure. To prove this, Table 1 shows that the compression ratio is 21.1%. As evidenced in Table 1, the crook degree and the adhesion strength shows that below 20 MPa, the pole piece has a very limited crook degree and insufficient adhesion strength, resulting in bad flexibility, cracks, or even fall off of the active substance upon winding. Consequently, capacitors made of such electrode have poor recycling performance and faster attenuation of specific capacity. When a capacitor which had undergone 1,000 charge−discharge cycles was dismantled, the fall off of carbon powder was seen in varying degrees. Consequently, 20 MPa was determined as the optimal manufacturing pressure with the most positive influence on performance.

Table 2 Performances of supercapacitors with electrodes of various molding pressures

Pressure (MPa)	Mass specific capacitance, C_p (Fg^{-1})	Volume specific capacitance, C_v ($F\ cm^{-3}$)	Energy density, E_p ($Wh\ kg^{-1}$)	Maximum power density, P_{max} ($kW\ kg^{-1}$)	Internal resistance, R (Ω)	Charging/discharging, efficiency η (%)
5	327.2	166.6	2.1	9.7	3.1	85.7
10	348.6	174.8	2.3	10.7	2.3	91.4
15	359.9	179.8	2.6	11.2	1.8	95.8
20	370.0	185.2	2.9	12.4	1.0	97.6
25	342.1	171.1	1.8	10.2	1.2	90.2

Table 3 Performances of supercapacitors with electrodes of various molding temperature

Temperature °C	Mass specific capacitance, C_p (Fg^{-1})	Volume specific capacitance, C_v ($F\ cm^{-3}$)	Energy density, E_p ($Wh\ kg^{-1}$)	Maximum power density, P_{max} ($kW\ kg^{-1}$)	Internal resistance, R (Ω)	Charging/discharging, efficiency, η (%)
25	332.7	165.9	1.7	9.8	1.8	88.9
50	353.3	173.1	2.1	10.6	1.4	90.3
80	370.0	185.2	2.9	12.4	1.0	97.6
100	352.4	173.1	2.3	11.0	1.2	96.8
120	331.2	165.2	2.0	10.9	1.3	95.6

Influence of electrode molding temperature

The electrodes molded after being rolled and compressed for 60 s under 20 MPa in different temperatures were assembled into a simulated supercapacitor. The relevant electrochemical tests were conducted, and the functional parameters of the supercapacitor were calculated based on the constant current charge–discharge curve and formulas (Table 3). At 80 °C pole piece molding temperature, the supercapacitor exhibits the best performance.

Electrode molding temperature is another important factor which influences specific capacity and internal resistance. Cold pressing techniques could not fully extend the molecular chain of the adhesion agent, hindering the agent from fully moisturizing the aluminum surface and resulting in less than enough adhesion strength. In contrast, hot pressing techniques could enable the molecular chain of the adhesion agent to fully extend and adhere to the aluminum surface with greater strength. Higher temperatures result in better dispersant reaction to the conductive additive, so that the latter becomes more evenly distributed within the electrode, improving conductivity and specific capacity as well as decreasing internal resistance. However, extremely high temperatures could cause demulsification of the thickening agent and the adhesion agent, thus inflicting partial vitrification and consequent adhesion deterioration. Table 1 shows that at molding temperatures below 80 °C (ET_6 25 °C and ET_7 50 °C), the pole piece has poor mechanical properties: the crook degree and the adhesion strength are even not up to standard. The active substance of the electrode falls off to varying degrees in winding and testing processes, and the specific capacity decreased accordingly. In contrast, when the temperature was higher than 80 °C (ET_8 100 °C and ET_9 120 °C), the electrode adhered to the sheeting machine and suffered damages, which is also undesirable. At 80 °C, the flexibility and the adhesion strength are both up to standard. Upon winding, no noticeable fall off of the active substance occurred. As the temperature rose, the specific capacity increased dramatically, so did the energy intensity, but the internal resistance decreased (Table 3). At temperatures greater than 80 °C, some active substance fell off and adhered to the sheeting machine, the electrical capacity dropped quickly, the internal resistance rose, and the recycling performance became undesirable. Therefore, at 80 °C, the supercapacitor has the best performance.

Influence of electrode molding time

Electrode molded at 20 MPa at 80 °C under different rolling and pressing times were assembled into a simulated supercapacitor. The electrochemical impedance, cyclic voltammetry, and constant current charge and discharge tests were conducted. The functional parameters were listed in Table 4, which shows that when the time for hot press molding was short (ET_{10}, 30 s), the active substance cannot fully contact with the aluminum sheets, resulting in an internal resistance of 1.6 Ω. When the molding time was 60 s (EP_4), the internal resistance was 1.0 Ω, indicating a dramatic drop and a surge of electrical capacity as well. However, when the molding time kept increasing (ET_{11}, 120 s), the internal resistance rose to 1.2 Ω and the specific

Table 4 Performances of supercapacitors with electrodes of various molding time

Time (s)	Mass specific capacitance, C_p (Fg^{-1})	Volume specific capacitance, C_v ($F\ cm^{-3}$)	Energy density, E_p ($Wh\ kg^{-1}$)	Maximum power density, P_{max} ($kW\ kg^{-1}$)	Internal resistance, R (Ω)	Charging/discharging, efficiency η (%)
30	342.7	171.6	2.4	10.9	1.6	89.4
60	370.0	185.2	2.9	12.4	1.0	97.6
120	356.8	178.4	2.6	11.4	1.2	94.9

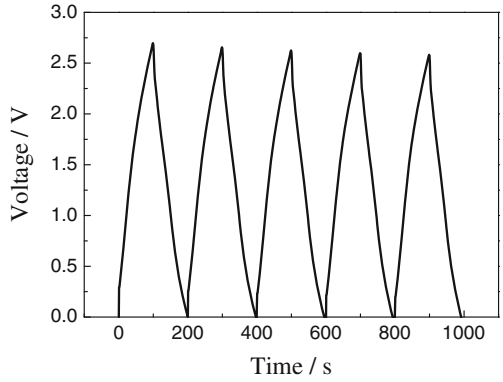

Fig. 2 Constant current charge–discharge curves at current of 200 mA

capacity also fell. This may be because the rolling and pressing time was too long, resulting in a very high compression ratio (23.2%) of the active carbon micro holes, as shown in Table 1. The electrolyte could not penetrate the internal electrode and the internal resistance rose, resulting in a low utilization rate of the active substance and a drop in specific capacity. Therefore, at 60 s, the supercapacitor has the best performance.

The electrochemical performance of the supercapacitor with optimum technology

Constant current charging/discharging

One thousand charge–discharge tests at 200 mA were performed on a supercapacitor with optimum conditions, as shown in Fig. 2. At molding conditions 20 MPa, 80 °C, and 60 s (EP_4), the capacitor had a much smaller voltage [20] (caused by the internal resistance at the moment of charge–discharge initiation) than those of the electrodes made under other conditions, indicating smaller internal resistance of the supercapacitor. The charge–discharge efficiency of the supercapacitor was calculated as 97.6%.

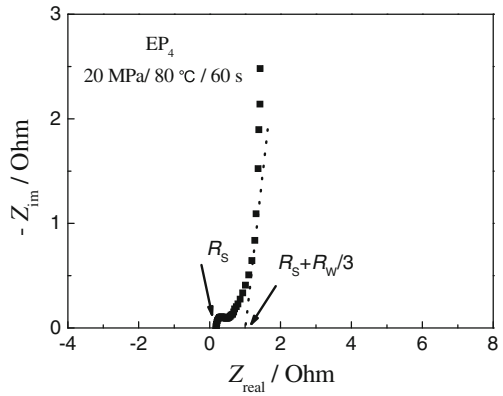

Fig. 3 Nyquist diagram of supercapacitor

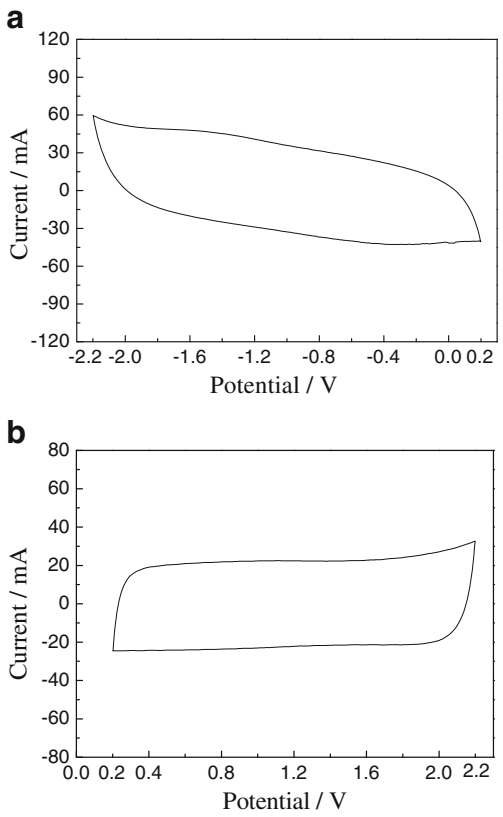

Fig. 4 **a** Cyclic voltammograms of the anode; **b** cyclic voltammograms of the cathode

AC impedance

An ideal supercapacitor requires characteristics which enable it to be regarded as a series connection between resistance and capacitor. The Nyquist plot shows that the actual impedance remained unchanged, but the capacity reactance gradually rose as the frequency decreased, forming a straight line vertical to the real axis [21]. The actual Nyquist curve of the supercapacitor has a certain slope. Figure 3 reveals that the medium and low frequency area is similar to that of an ideal capacitor.

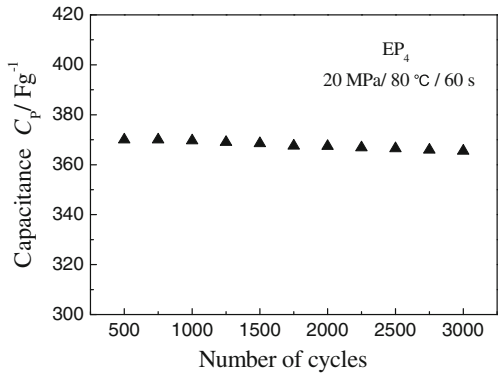

Fig. 5 Cycle life of supercapacitor

Besides this, the supercapacitor also has the typical characteristics of a capacitor, which are also identical to the impedance characteristics of supercapacitors described in literature [22]. The electrical resistance can be obtained by the high-frequency intercept with the horizontal axis, which consists of R_s (the internal resistance of the solution) and R_w (the internal resistance of the active carbon hole). The magnitude of equivalent series resistance ($R_s+R_w/3$) can be obtained from the tangent of the Nyquist plot in the Fig. 3 for carbon-based electrode; the internal resistance of the supercapacitor is about 1.0 Ω.

Cyclic voltammetry

A progressive scanning method (v=5 mV s^{-1}) was adopted in the cyclic voltammetry test. Figure 4a shows the cyclic voltammetry curve of the negative electrochemical threshold, whereas Fig. 4b shows the cyclic voltammetry curve of the positive electrochemical threshold. The figures show that the negative electrochemical threshold is 2.4 V and the positive electrochemical threshold is 2.0 V. The electrochemical windows for the supercapacitor could be high at 4.4 V. The cyclic voltammetry curve did not show noticeable reaction peaks but standard rectangles within the investigated electrochemical window, similar to that of an ideal supercapacitor [23]. The results indicate that the electrolyte did not react with the electrode material, the spectrum, the current collector, or any other component, indicating it had good reversibility, typical capacitance performance, and satisfied chemical stability [24].

Cycle life

Figure 5 shows the curve of the capacitance retention percentage of the supercapacitor changing with the 3,000 charge–discharge cycles from 1.5 to 3.0 V. The capacitance attenuation was 1.2% and remained constant, indicating that the supercapacitor has a stable charge–discharge performance and cyclic lifespan. Also, the results showed that the ability of the supercapacitor to work for a long time period under a working voltage of 2.7 V.

Conclusions

The molding technique to prepare supercapacitor was investigated in this study. The electrochemical performance of the supercapacitor was examined using an AC impedance, a cyclic voltammetry, and constant current charging/discharging tests. According to the results, at 20 MPa and 80 °C for 60 s, the supercapacitor showed the best performances with its electrochemical window reaching 4.4 V, a charge–discharge efficiency of 97.6%, and a specific capacitance of 370.0 Fg^{-1}.

Acknowledgment This work was supported by the Natural Science Foundation of China (No. 21003081) and the Key Laboratory Foundation of Liaoning Province of China (No. LS2010001).

References

1. Campana FP, Hahn M, Foelske A, Ruch P, Kötz R, Siegenthaler H (2006) Electrochem Commun 8:1363–1365
2. Lazzari M, Soavi F, Mastragostino M (2009) J Electrochem Soc 156:661–665
3. Leitner KW, Winter M, Besenhard JO (2003) J Solid State Electrochem 8:15–16
4. Cai KD, Mu WF, Zhang QG Jin ZX, Wang DL (2010) Electrochem Solid State Lett A147–A149
5. Wang YG, Cheng L, Xia YY (2006) J Power Sources 153:191–196
6. Yokoyama Y, Shimosaka N, Matsumoto H (2008) Electrochem Solid State Lett 11:A72–75
7. Cheng L, Li HQ, Xia YY (2006) J Solid State Electrochem 10:405–410
8. Balducci A, Dugas R, Taberna PL, Simon P, Plée D, Mastragostino M, Passerini S (2007) J Power Sources 165:922–926
9. Kuo SL, Wu NL (2005) Electrochem Solid State Lett 8:A495–498
10. Hardwick LJ, Hahn M, Ruch P (2006) Electrochim Acta 52:675–679
11. Rajeswari J, Kishore PS, Viswanathan B, Varadarajan TK (2009) Electrochem Commun 11:572–575
12. Zhang LL, Zhao XS (2009) Chem Soc Rev 38:2520–2531
13. Vix CG, Saadallah S (2004) Mater Sci Eng 108:148–155
14. Kotz R, Carlen M (2000) Electrochim Acta 45:2483–2498
15. Arulepp M, Permann L, Leis J (2004) J Power Sources 133:320–328
16. Frackowiak E (2007) Phys Chem Chem Phys 9:1774–1785
17. Show Y, Imaizumi K (2007) Diamond Relat Mater 16:154–158
18. Zeng YQ, Li BH, Zhou BW (2005) New Carbon Mater 20:299–303
19. Qu D, Shi H (1998) J Power Sources 74:99–107
20. Sivaraman P, Thakur A, Kushwaha RK, Ratna D, Samui AB (2006) Electrochem Solid State Lett 9:435–438
21. Bohlen O, Kowal J, Sauer DU (2007) J Power Sources 172:468–475
22. Wang Y, Shi ZQ, Huang Y, Ma YF, Wang CY, Chen MM, Chen YS (2009) J Phys Chem C 113:13103–13107
23. Li Q, Zuo XX, Liu JS, Xiao X, Shu D, Nan JM (2011) Electrochim Acta 58:330–335
24. Lai YQ, Chen XJ, Zhang ZA, Li J, Liu YX (2011) Electrochim Acta 56:6426–6430